Links between iron supply, marine productivity, sea surface temperature, and CO_2 over the last 1.1 Ma

Alfredo Martínez-Garcia,[1] Antoni Rosell-Melé,[1,2] Walter Geibert,[3,4,5] Rainer Gersonde,[6] Pere Masqué,[1] Vania Gaspari,[7] and Carlo Barbante[7,8]

Received 3 July 2008; revised 9 October 2008; accepted 27 October 2008; published 14 February 2009.

[1] Paleoclimatic reconstructions have provided a unique data set to test the sensitivity of climate system to changes in atmospheric CO_2 concentrations. However, the mechanisms behind glacial/interglacial (G/IG) variations in atmospheric CO_2 concentrations observed in the Antarctic ice cores are still not fully understood. Here we present a new multiproxy data set of sea surface temperatures (SST), dust and iron supply, and marine export productivity, from the marine sediment core PS2489-2/ODP Site 1090 located in the subantarctic Atlantic, that allow us to evaluate various hypotheses on the role of the Southern Ocean (SO) in modulating atmospheric CO_2 concentrations back to 1.1 Ma. We show that Antarctic atmospheric temperatures are closely linked to changes in SO surface temperatures over the last 800 ka and use this to synchronize the timescales of our marine and the European Project for Ice Coring in Antarctica (EPICA) Dome C (EDC) records. The close correlation observed between iron inputs and marine export production over the entire interval implies that the process of iron fertilization of marine biota has been a recurrent process operating in the subantarctic region over the G/IG cycles of the last 1.1 Ma. However, our data suggest that marine productivity can only explain a fraction of atmospheric CO_2 changes (up to around 40–50 ppmv), occurring at glacial maxima in each glacial stage. In this sense, the good correlation of our SST record to the EDC temperature reconstruction suggests that the initial glacial CO_2 decrease, as well as the change in the amplitude of the CO_2 cycles observed around 400 ka, was most likely driven by physical processes, possibly related to changes in Antarctic sea ice extent, surface water stratification, and westerly winds position.

Citation: Martínez-Garcia, A., A. Rosell-Melé, W. Geibert, R. Gersonde, P. Masqué, V. Gaspari, and C. Barbante (2009), Links between iron supply, marine productivity, sea surface temperature, and CO_2 over the last 1.1 Ma, *Paleoceanography*, *24*, PA1207, doi:10.1029/2008PA001657.

1. Introduction

[2] The causes of the glacial/interglacial (G/IG) variations in atmospheric CO_2 concentrations observed in the Antarctic ice cores [*Luthi et al.*, 2008; *Petit et al.*, 1999; *Siegenthaler et al.*, 2005] are still under debate. It is likely that the full 80–100 ppmv range of fluctuations in atmospheric CO_2 can only be successfully explained by a combination of physical and biogeochemical mechanisms that are involved in the regulation of the oceanic carbon reservoir [*Abelmann et al.*, 2006; *Francois et al.*, 1997; *Kohler et al.*, 2005; *Sigman and Boyle*, 2000; *Sigman et al.*, 2004; *Stephens and Keeling*, 2000; *Toggweiler et al.*, 2006].

[3] The process of iron fertilization of marine biota [*Martin*, 1990] has received significant attention in recent years, both as a driver of CO_2 during G/IG cycles [*Kohfeld et al.*, 2005; *Kohler et al.*, 2005; *Watson et al.*, 2000] and in the context of mitigation strategies to counteract anthropogenic CO_2 emissions [*Buesseler and Boyd*, 2003; *Chisholm et al.*, 2001, 2002; *Johnson and Karl*, 2002]. According to the iron hypothesis [*Martin*, 1990], an increase in the atmospheric supply of iron by dust during glacial periods, may have stimulated marine productivity in the high-nutrient low-chlorophyll (HNLC) regions (mainly the Southern Ocean, and the North and Equatorial Pacific), contributing to the reduction of atmospheric CO_2 concentrations. The effect of iron on marine ecosystem structure and productivity has been proven by a series of short-term in situ iron enrichment experiments, but also by observations of phytoplankton blooms induced by natural iron fertilization [*Blain et al.*, 2007; *Boyd et al.*, 2007]. While the efficacy of artificial iron experiments to sequester organic carbon to the deep ocean is still under controversial discussion [*Buesseler et al.*, 2008], the study of natural iron fertilization results in a significant increase in carbon export with increasing iron supply [*Blain et al.*, 2007]. Paleoceano-

[1]Institut de Ciència i Tecnologia Ambientals, Universitat Autònoma de Barcelona, Bellaterra, Catalonia, Spain.
[2]Institució Catalana de Recerca i Estudis Avançats, Barcelona, Catalonia, Spain.
[3]School of Geosciences, University of Edinburgh, Edinburgh, UK.
[4]Dunstaffnage Marine Laboratory, Scottish Association for Marine Science, Oban, UK.
[5]Formerly at the Alfred Wegener Institute for Polar and Marine Research, Bremerhaven, Germany.
[6]Alfred Wegener Institute for Polar and Marine Research, Bremerhaven, Germany.
[7]Institute for the Dynamics of Environmental Processes, CNR, Venice, Italy.
[8]Department of Environmental Sciences, University Ca'Foscari of Venice, Venice, Italy.

0883-8305/09/2008PA001657$12.00

graphic and model results indicate that increased iron availability could explain up to one half of the observed CO_2 drawdown in the last glacial period [*Gaspari et al.*, 2006; *Kohfeld et al.*, 2005; *Watson et al.*, 2000].

[4] Recent modeling studies have shown that the full G/IG atmospheric CO_2 variability could only be explained by considering several physical processes driven by the complex interaction among sea ice cover, surface water stratification and the position of the westerly winds around Antarctica [*Francois et al.*, 1997; *Kohler et al.*, 2005; *Sigman et al.*, 2004; *Stephens and Keeling*, 2000; *Toggweiler et al.*, 2006]. According to this view, during glacial stages cold temperatures promoted an expansion of the Antarctic sea ice cover, inducing stratification of the polar ocean, limiting ocean ventilation, and allowing more carbon to be trapped in the deep ocean [*Francois et al.*, 1997; *Sigman and Boyle*, 2000; *Stephens and Keeling*, 2000]. The northward migration of the westerly winds associated with cold glacial temperatures acted as a positive feedback, preventing the upwelling of CO_2-rich deep waters around Antarctica, and contributing further to the isolation of the deep ocean from the atmosphere that kept atmospheric CO_2 concentrations low during glacial stages [*Toggweiler*, 1999; *Toggweiler et al.*, 2006; *Toggweiler and Russell*, 2008].

[5] Understanding the interplay between these mechanisms through time is thus of crucial importance to gauge their effect on atmospheric CO_2. However, little is known about their evolution beyond the last two glacial stages. The paleoclimatic reconstruction from the Antarctic ice cores generated by the European Project for Ice Coring in Antarctica (EPICA) community provided a unique record of atmospheric CO_2 concentrations [*Luthi et al.*, 2008; *Petit et al.*, 1999; *Siegenthaler et al.*, 2005], and also the opportunity to assess the role of iron supply, sea ice extent and wind intensity on the marine carbon cycle over the last eight glacial cycles [*Wolff et al.*, 2006]. However, ice core records only allow indirect inference of these processes in the marine realm, and it is unlikely that they can be extended beyond their current time span in the near future.

[6] Here we present independent estimates of iron and dust supply, marine productivity and sea surface temperature (SST) over the last 1.1 Ma from a deep-sea sediment record (PS2489-2/ODP Site 1090) located in the subantarctic South Atlantic (Figure 1). The region studied is particularly influential for the marine carbon reservoir through changes in westerly winds position [*Toggweiler et al.*, 2006] and iron fertilization of marine biota [*Brovkin et al.*, 2007; *Kohfeld et al.*, 2005]. Moreover, SST changes at this site are strongly influenced by the movements of the isotherms related to the Antarctic Circumpolar Current (ACC) frontal system which, in fact, determine the extension of the Antarctic sea ice cover during the G/IG cycles through the Pleistocene [*Gersonde et al.*, 1999]. We discuss the marine data in combination with a new high-resolution record of terrestrial iron supply from the EPICA Dome C (EDC) ice cores. At the marine site a combination of organic and inorganic proxies allows us to quantify iron and dust fluxes, as well as their effect on marine productivity, in the same sedimentary record. In this sense, the data set represents a marine counterpart of the EDC record over the last 800 ka, and provides new information on past changes in SST, dust and iron supply and marine productivity back to 1.1 Ma, allowing us to assess the role of marine processes in modulating atmospheric CO_2 concentrations through time.

2. Material and Methods

2.1. Site Location and Core Material (PS2489-2/ODP Site 1090)

[7] ODP Site 1090 (42°54.8′S, 8°53.9′E) was recovered during ODP Leg 177 in the central part of the Subantarctic Zone at 3700 m water depth (Figure 1). In order to obtain a continuous record of the Pleistocene, samples from the nearby core PS2489-2 (42°52.4′S, 8°58.4′E) were analyzed for the interval from 0 to 500 ka, following the approach described by *Becquey and Gersonde* [2002]. Sediment cores were sampled at a resolution of 1–5 ka for core PS2489-2 and 2 ka for ODP Site 1090. The interval of overlap of the two cores is indicated in Figure 2 and shown in detail in the online Auxiliary Material.[1] No significant differences were found in SST, biomarkers concentrations and MAR in this interval between the two cores (see Figure S1 of the Auxiliary Material). The composite record is referred in the text as site PS2489-2/ODP1090.

2.2. Age Model

[8] The initial age model for PS2489-2 [*Becquey and Gersonde*, 2003] and ODP Site 1090 [*Venz and Hodell*, 2002] was generated by benthic oxygen isotopes correlation, and it is used in Figure 2. In Figures 3–7 we use a new age model modified by graphic correlation of our alkenone-based SST to the ice core temperature reconstruction from the EPICA project [*Jouzel et al.*, 2007], using the new EDC3 chronology [*Parrenin et al.*, 2007] and the software Analyseries [*Paillard et al.*, 1996]. This allows for direct comparison of the continental and marine records in the same timescale. Nonetheless, the correlation of the SST and the atmospheric temperature from EDC is good before this adjustment of the age model, as evidenced by the good agreement between the $\delta^{18}O$ of PS2489-2/ODP1090 and the Lisieky and Raymo (LR) stack (Figure 2a). Depth/age pointers for site PS2489-2/ODP1090 obtained after the correlation of the two records are available in Table S1 of the online Auxiliary Material.

2.3. Biomarkers Analysis

[9] The method employed for biomarkers analysis has been described in detail elsewhere [*Kornilova and Rosell-Mele*, 2003; *McClymont et al.*, 2007]. Briefly, sediment samples were freeze-dried, homogenized, and 1–5 g of sediment were microwave extracted. Organic extracts were analyzed using a Thermo Trace gas chromatogram fitted with a flame ionization detector, in splitless injection mode, using helium as carrier gas (1.5 ml/min constant flux). Chromatographic separation of the organic compounds was achieved using an Agilent HP-1 capillary column of 60 m length, 0.25 mm internal diameter, and 0.25 μm film thickness, fitted to a 5 m precolumn. The oven temperature

[1] Auxiliary materials are available in the HTML. doi:10.1029/2008PA001657.

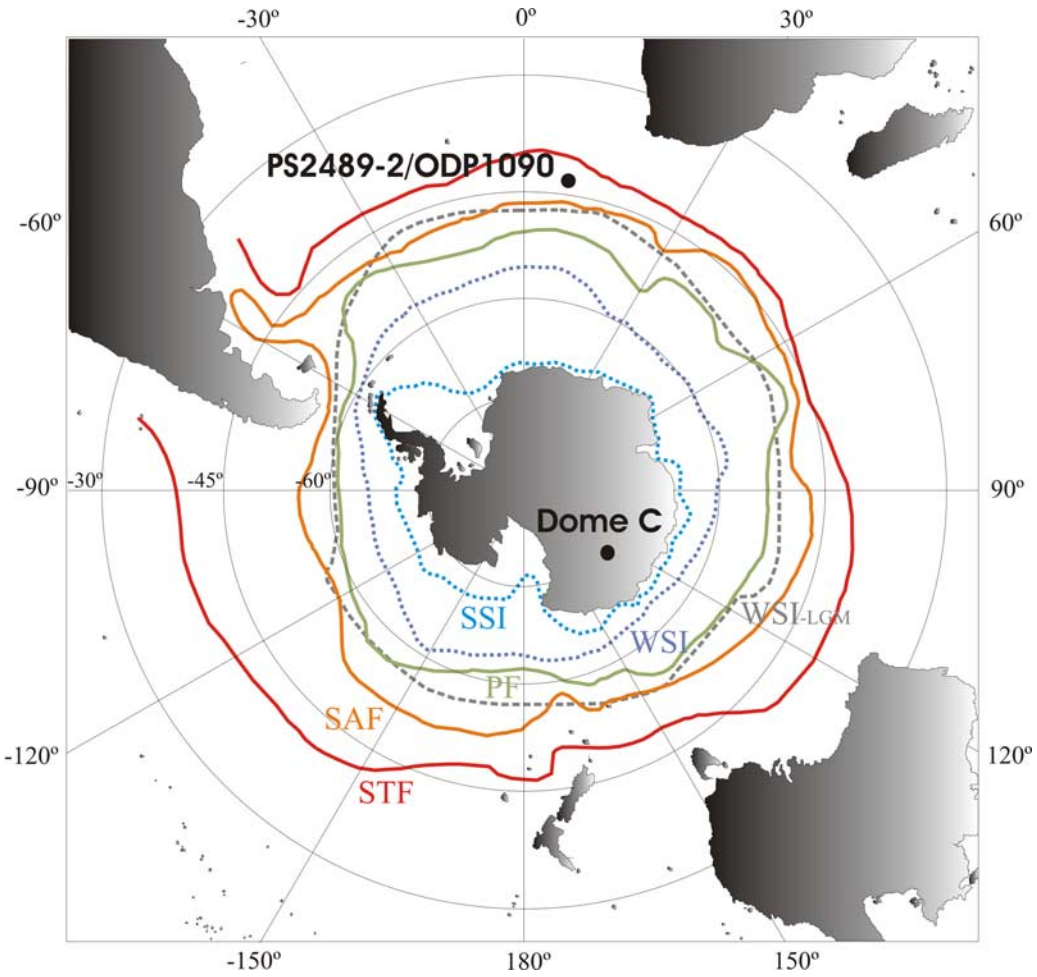

Figure 1. Location of Site PS2489-2/ODP1090 and European Project for Ice Coring in Antarctica (EPICA) Dome C ice record. Solid lines indicate the present-day position of the different oceanic fronts according to *Belkin and Gordon* [1996]. Dashed blue lines correspond to modern sea ice boundaries according to *Comiso* [2003]. Dashed gray line represents Last Glacial Maximum (LGM) winter sea ice edge reconstruction according to *Gersonde et al.* [2005]. STF, Subtropical Front; SAF, Subantarctic Front; PF, Polar Front; WSI, Winter Sea Ice; SSI, Summer Sea Ice; WSI_{LGM}, Winter Sea Ice during the LGM.

was programmed to be held at 80°C for 1 min, then increased at 20°C/min to 120°C, at 6°C/min until 320°C, and held for 20 min. The identification of the different compounds was achieved through comparison of the chromatographic relative retention times of the target compounds with standards. Several selected samples were analyzed by mass spectrometry to confirm peak identities and the absence of coeluting peaks.

[10] To estimate SST the U^{K}_{37} paleotemperature index [*Brassell et al.*, 1986; *Prahl and Wakeham*, 1987] is used in preference to $U^{K}_{37}{}'$ in this study as it has been shown to be better correlated to annual mean SST in high latitudes [*Bard et al.*, 2000; *Bendle and Rosell-Mele*, 2004; *Rosell-Mele et al.*, 1995; *Rosell-Mele*, 1998]. The reproducibility of the procedure was evaluated using a homogeneous sediment standard, extracted with every batch of 14 samples. The relative analytical errors were below 0.5°C in SST estimates and below 10% in the determination of n-alkanes and alkenones concentration, which is within the range of the analytical error of the method [*Rosell-Mele et al.*, 2001].

2.4. Multielemental Analysis

[11] Fe, Al, U, ^{232}Th, U, and Re concentrations were determined on 50 mg of freeze-dried sediment, digested in a pressure-assisted microwave system using 3 ml of subboiling distilled HNO_3, 2 ml of suprapur® HCl and 0.5 ml of suprapur® HF, together with the isotopic spikes for isotope dilution measurement of U and Th (see section 2.5). The sediment and acid mixture were placed in microwave vessels and kept closed at 205°C during 40 min. Afterward, samples were taken to dryness by gentle heating in the microwave using an evaporation accessory connected to a vacuum pump. The near dry samples were redissolved in 5 ml HNO_3 and heated to 160°C. After a volumetric dilution to 50 ml, a subsample of 5 ml together with Rh as an internal standard was further diluted to 50 ml for the

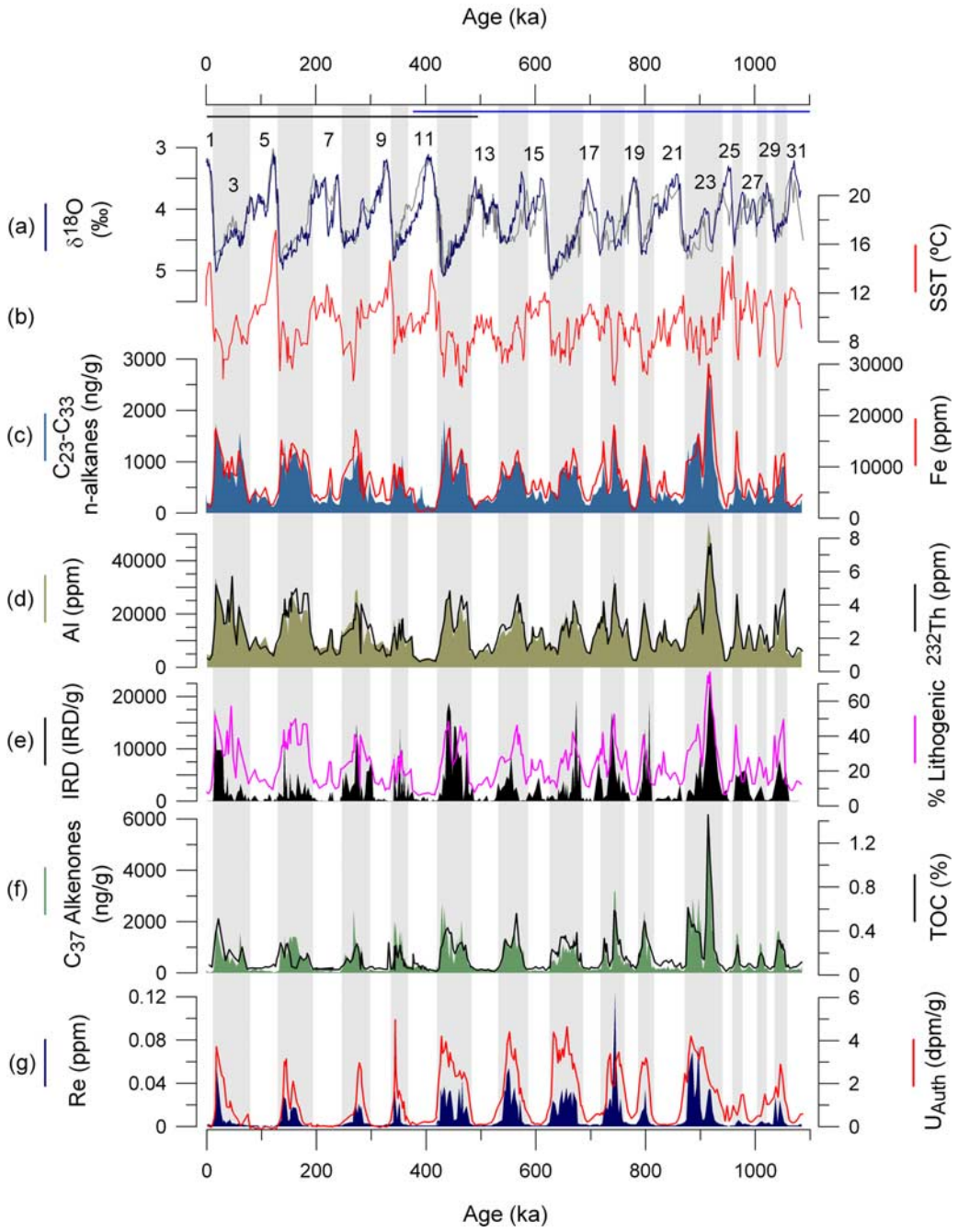

Figure 2. Organic and inorganic tracers concentration at Site PS2489-2/ODP1090. (a) Lisiecki and Raymo (LR) δ^{18}O global stack (blue) [*Lisiecki and Raymo*, 2005] and PS2489-2/ODP1090 δ^{18}O (gray) [*Becquey and Gersonde*, 2003; *Venz and Hodell*, 2002]. Marine Isotope Stages (MIS) are shown for reference. (b) Alkenone sea surface temperature (SST). (c) Long-chain odd carbon-numbered n-alkanes (C_{23-33}) concentration (blue) and iron concentration (red). (d) Al (brown) and ^{232}Th (black) concentration. (e) Ice rafted debris IRD (black) [*Becquey and Gersonde*, 2002] and percentage of lithogenic material (magenta). (f) C_{37} alkenones concentration (green) and percentage of total organic carbon (TOC) (black) [*Diekmann and Kuhn*, 2002]. (g) Re (blue) and authigenic U (red) concentrations. Shaded areas highlight high-productivity intervals when alkenones concentration and TOC start to increase from the interglacial value. Black and blue lines on top of the Figure 2 show the intervals covered by PS2489-2 and ODP Site 1090 samples, respectively. Age model according to *Venz and Hodell* [2002].

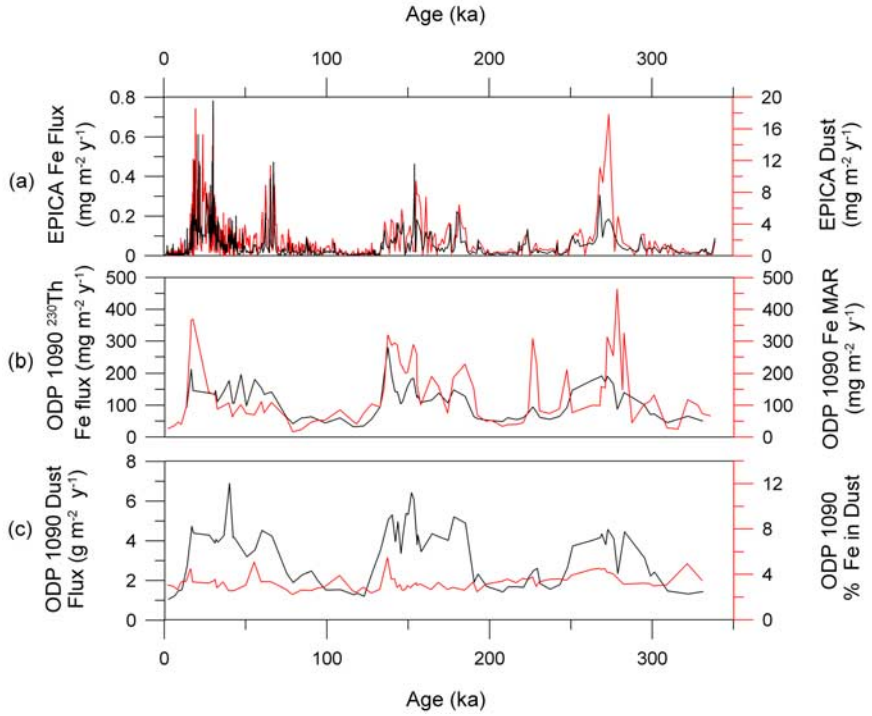

Figure 3. Marine versus terrestrial dust and Fe fluxes over the last 330 ka. (a) EPICA Dome C Fe flux (black) and dust flux (red) [*EPICA Community Members*, 2004]. (b) PS2489-2/ODP1090 ^{230}Th-normalized Fe flux (black) and Fe mass accumulation rate (MAR) (red). (c) PS2489-2/ODP1090 ^{230}Th-normalized dust flux (black) and percent of iron in dust (red). The age model was obtained by correlation of marine and continental temperature profiles (see section 2.2).

multielement analysis by Inductively Coupled Plasma Sector-Field Mass Spectrometry (ICP-SFMS, Element2, Thermo Scientific). Sensitivity was increased using an APEX Q desolvation system (typically about 2,000,000 cps/ppb for U at a nominal flow rate of 100 μL sample @ 1275 W plasma power). All calibrations were done with dilutions of certified standard solutions. External reproducibility was evaluated using the NIST standard reference material 2702 (inorganics in marine sediment), except for Re. With each batch of samples, two procedural blanks were run. Abundant elements (Al and Fe) were analyzed in high resolution and detected in the "analog" counting mode. The remaining elements reported here were measured in low-resolution mode, and detected by ion counting (Re) or in the automatically cross-calibrated "both" mode (analog or ion counting, depending on count rate). Average relative errors for Fe and Al were 1.8 and 2.1% (1σ), respectively. External reproducibility for Fe in NIST 2702 was 5.6% and, due to very high concentrations in the reference material, only 15% for Al. The reported concentrations for uranium and thorium samples younger than 330 ka were obtained by isotope dilution (see section 2.5).

2.5. Thorium and Uranium Isotopes Analysis

[12] The remaining volume of the full digested solution was used for the measurement of uranium and thorium isotopes by isotope dilution (only samples within the interval 0–330 ka). ^{229}Th and ^{236}U spikes were added prior to the microwave digestion of the sample. The solution was treated with three successive steps of iron precipitations, which retain Th and U but remove most of the other metals. The precipitate was redissolved in HNO_3 (3 M). Afterward, Fe, Th, and U were separated using 2 ml columns filled with UTEVA® resin. Prior to column separation, 250 μL of a 1 M aluminum nitrate solution was added to the sample to prevent the effect of matrix components (mainly phosphates) on UTEVA® resin efficiency. Added aluminum can effectively tie up the phosphate preventing its interference with Th uptake by the resin [*Horwitz et al.*, 1992]. The eluted Th and U fractions were heated to near dryness and redissolved in 8 M HNO_3 twice. Afterward, the two fractions were dissolved in 1 M HNO3 and analyzed by ICP-SFMS in low-resolution mode (1200 W plasma power, nominal flow rate 100 μL via APEX Q desolvation system). ^{229}Th and ^{230}Th were measured by ion counting, ^{232}Th in analog mode (automatically cross-calibrated with the counting mode). All U isotopes were measured in ion counting mode, except ^{238}U, which was calculated from ^{235}U. Adequate corrections were applied to account for tailing from ^{232}Th, as monitored by the masses 231.5 and 230.5. Mass bias of the instrument was monitored externally by a solution of U in natural isotopic composition, supplied by the Physikalisch-Technische Bundesanstalt Braunschweig (PTB). Dead time correction (25 ns) was applied. For ^{230}Th, all results with less than 100 counts per second or 1 σ ratio error > 5% were discarded (typical count rates for

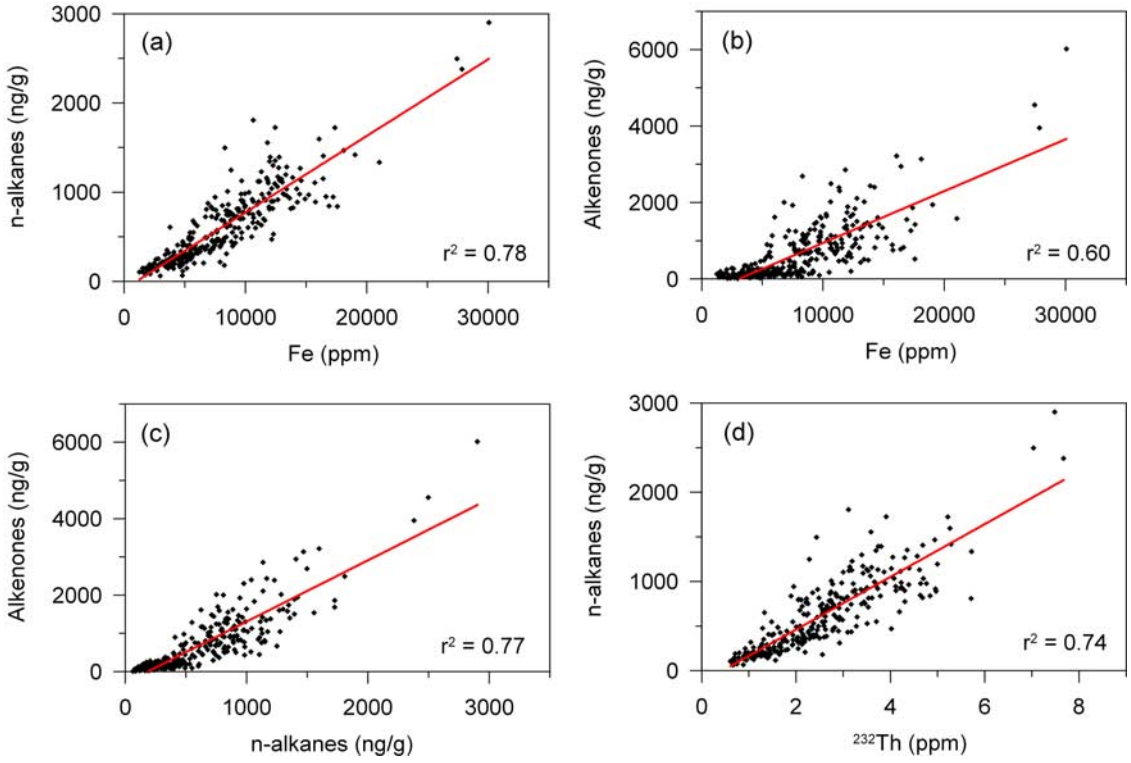

Figure 4. Linear regression between the concentrations of some elements measured at Site PS2489-2/ODP1090: (a) n-alkanes versus Fe, (b) alkenones versus Fe, (c) alkenones versus n-alkanes, and (d) n-alkanes versus ^{232}Th.

^{230}Th were 300–5000 cps for the samples, 10,000 cps for the standard). The external reproducibility of the method was evaluated by duplicate analysis of the UREM 11 standard reference material [*Hansen and Ring*, 1983], in each batch of 24 samples, and it was found to be overall 3% (1σ). The mean ^{230}Th activity found in UREM 11 was 43.60±1.31 dpm/g (1σ), n = 13.

2.6. Flux Calculations and Associated Errors

[13] $^{230}Th_{ex}$ was calculated according to *Francois et al.* [2004], using a $^{232}Th/^{238}U$ activity ratio of 0.4, and a $^{234}U/^{238}U$ activity ratio in the lithogenic end-member of 0.9. In absence of complicating factors such as large postdepositional sediment redistribution or sediment inputs from shallower depths, $^{230}Th_{ex}$ can be readily converted into preserved vertical mass fluxes of a specific sedimentary compound [*Francois et al.*, 2004; *Frank et al.*, 2000; *Geibert et al.*, 2005]. Taking into account some potential variability of the lithogenic ^{232}Th signal (7 ppmv–13 ppmv), analytical errors in some $^{230}Th_{ex0}$ of up to 35%, as well as potential deviations from constant vertical ^{230}Th flux at this location, we are confident that actual lithogenic fluxes are within 50% of the reported values for the ^{230}Th-normalized data (to 330 ka). Beyond this age, $^{230}Th_{ex}$ is not applicable owing to ^{230}Th decay and the increasing uncertainty of the method (see Figure S2 of the Auxiliary Material).

2.7. Fe Determination in EPICA Dome C Ice Cores

[14] As the ice cores are often contaminated for various metals on the outside due to the drilling fluid and core handling, each 5-cm-long section of an ice core was decontaminated by three repeated washings in ultrapure Milli-Q water until ~60% of the original sample was melted off [*Delmonte et al.*, 2002]. This decontamination procedure resulted as being a good compromise in terms of efficiency, with respect to the more strictly chiselling decontamination method for iron [*Gabrielli et al.*, 2005].

[15] Dissolvable Fe concentrations were determined by means of Inductively Coupled Plasma Sector Field Mass Spectrometry, ICP-SFMS (Element2, Thermo Scientific), in melted samples at pH 1, after at least 24 h from acidification (HNO_3 Ultrapure, Romil, Cambridge, UK). Special care was given to resolve the interference of $^{40}Ar^{16}O$ on ^{56}Fe by taking advantage of the medium resolution capability ($m/\Delta m = 4000$) of the sector field mass spectrometer. An exhaustive description of working conditions and measurement parameters were previously reported elsewhere [*Barbante et al.*, 1997; *Planchon et al.*, 2001]. The external calibration curve method was used for the quantification of the metal, with concentrations in the standard solutions (ICUS-1616, Ultra Scientific, North Kingstown, USA) ranging from 5×10^{-4} to 50 ng g^{-1}. A typical precision of 15%, in terms of relative standard deviation, was extrapolated from the results obtained for selected samples only,

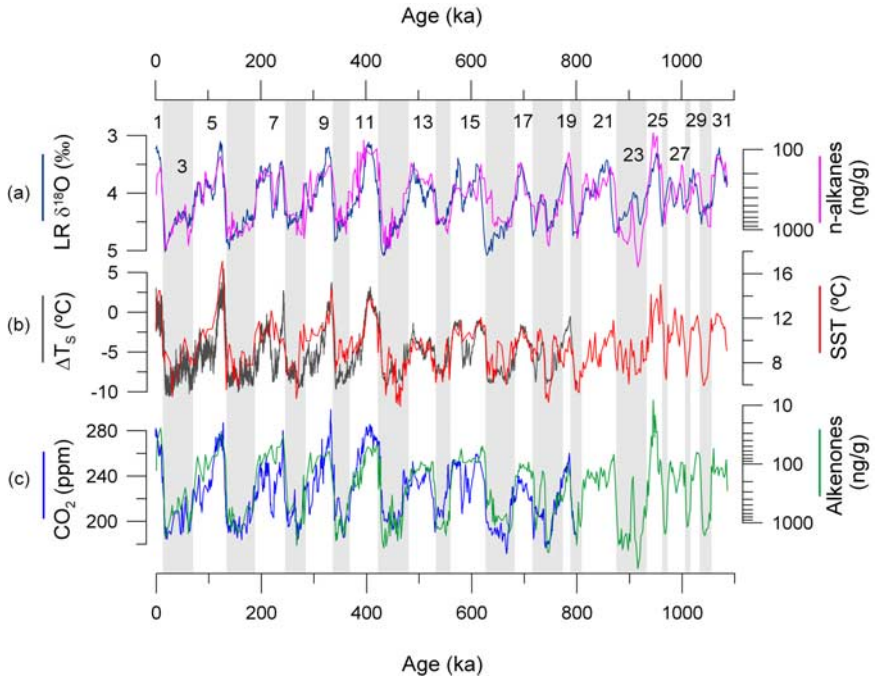

Figure 5. (a) Lisiecki and Raymo (LR) δ^{18}O global stack (blue) [*Lisiecki and Raymo*, 2005] and n-alkanes concentration from Site PS2489-2/ODP1090 (magenta). MIS are shown for reference. (b) Temperature reconstruction from EPICA ice cores (black) [*Jouzel et al.*, 2007] and alkenone-based SST from Site PS2489-2/ODP 1090 (red). (c) Atmospheric CO_2 concentration from the EPICA ice cores (blue) [*Luthi et al.*, 2008; *Petit et al.*, 1999; *Siegenthaler et al.*, 2005] and alkenones concentration from Site PS2489-2/ODP1090 (green). The age model was obtained by correlation of marine and continental temperature profiles (see section 2.2).

because of the very low volume available for all the samples. The element concentrations were converted in depositional fluxes by multiplying the elemental concentration by the water equivalent accumulation data estimated by *Parrenin et al.* [2007].

3. Results and Discussion

3.1. Dust and Iron Supply to the Subantarctic Atlantic

[16] Lithogenic fluxes through time are derived from the combined analysis of long chain odd-numbered n-alkanes, three inorganic tracers for lithogenic material (Al, Fe and ^{232}Th), and $^{230}Th_{ex}$ as an indicator of vertical mass flux. In deep-sea records, redistribution of bottom sediments can significantly alter vertical flux estimates. The ^{230}Th normalization method accounts for this process, and is used to convert concentrations of individual sedimentary compounds to their vertical fluxes [*Francois et al.*, 2004]. This enables us to determine vertically received lithogenic and iron fluxes at site PS2489-2/ODP1090 back to 330 ka. Beyond this age, $^{230}Th_{ex}$ is not applicable owing to ^{230}Th decay and increasing uncertainty (see section 2.6). Our data indicate relatively low sediment focusing in the record PS2489-2/ODP1090 during the last 330 ka (Figure 3). This contradicts the view that deep-ocean sediment recirculation is a significant source of iron to the SO sediments during glacial periods [*Latimer et al.*, 2006; *Latimer and Filippelli*, 2007]. Although this may influence drift sites [*Latimer and Filippelli*, 2007], it seems clear that this is not the case in other areas of the SO [*Kumar et al.*, 1995], such as that of PS2489-2/ODP1090. The close agreement between mass accumulation rates (MAR) and vertical fluxes in our record in the interval 0–330 ka, and their close correlation with EDC fluxes (Figure 3), justifies the assumption that MAR represents vertical fluxes in the older parts of the core.

[17] The distribution of n-alkanes in our record exhibits a clear predominance of long-chain odd carbon-numbered n-alkanes (i.e., CPI_{25-35} values between 3 and 9). This is representative of inputs of leaf waxes from terrestrial plants [*Eglinton and Hamilton*, 1967], which are commonly found in the organic fraction of eolian dust over the Atlantic Ocean [*Simoneit*, 1977]. Other significant sources of n-alkanes, such as from ice rafted debris (IRD) from the Antarctic continent and/or from the Patagonian ice sheet [*Hulton et al.*, 2002], are hence negligible as the geochemical signatures would correspond to mature organic material eroded by icebergs [*Rashid and Grosjean*, 2006; *Rosell-Mele et al.*, 1997], and the n-alkanes distribution would present a nonlong-chain odd carbon-numbered predominance (CPI values around 1). Therefore, we conclude that the n-alkanes in our record most likely reflect changes in the input of windborne continental material from South American sources.

[18] Al and Fe are elements associated with the lithogenic fraction of marine particles that provide independent estimates of the input of continental material [*Calvert and*

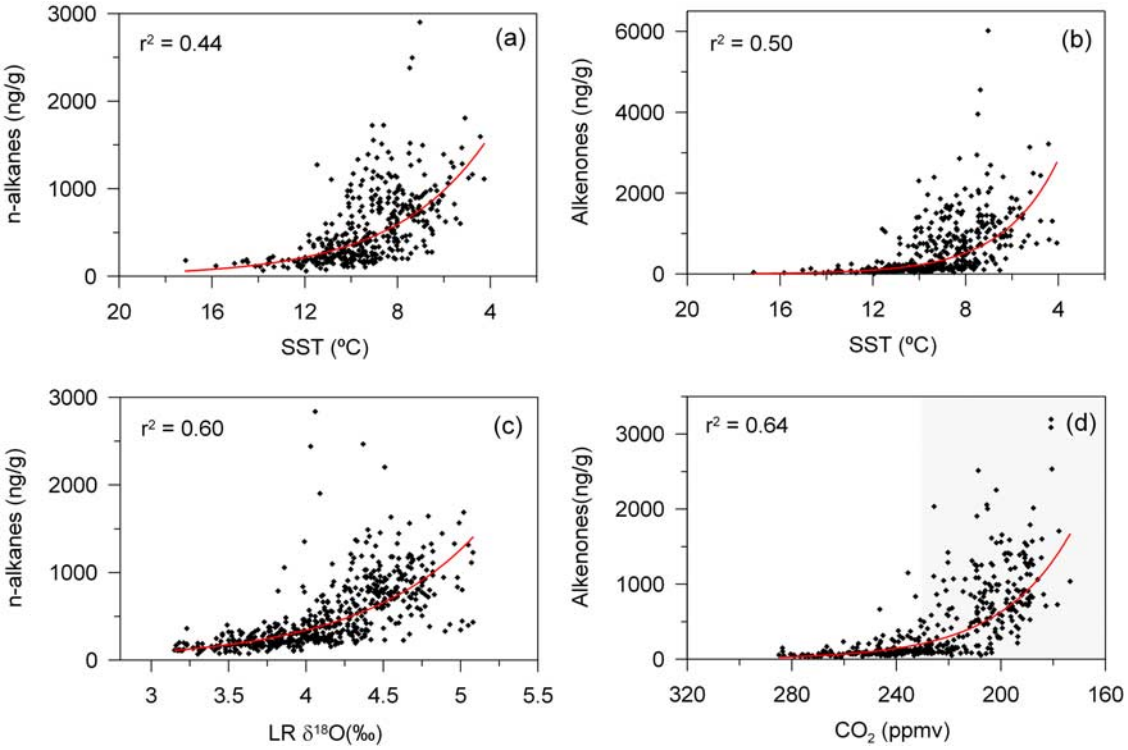

Figure 6. Exponential regression curves between (a) n-alkanes and SST, (b) alkenones and SST, (c) n-alkanes and global benthic $\delta^{18}O$ [*Lisiecki and Raymo*, 2005], and (d) alkenones and EPICA atmospheric CO_2 [*Luthi et al.*, 2008; *Petit et al.*, 1999; *Siegenthaler et al.*, 2005]. Figures 6a and 6b correspond to the regression of the two variables measured in the same samples of core PS2489-2/ODP1090. In the case of Figures 6c and 6d, given the differences in sampling resolution of the records, the series have been linearly interpolated to 2 ka before the regression. Shaded gray area in Figure 6d indicates values above 230 ppmv of CO_2.

Pedersen, 2007]. Moreover, ^{232}Th concentration can be used to assess quantitatively the fraction of lithogenic material in marine sediment cores (Figure 2e), as its concentration in lithogenic open ocean deposits is uniform at ~10 ppm [*Anderson et al.*, 2006; *Sayles et al.*, 2001; *Winckler et al.*, 2008]. The strong positive correlation observed between the concentrations and ^{230}Th corrected fluxes of inorganic tracers and n-alkanes over the entire record (e.g., Fe versus n-alkanes correlation, $r^2 = 0.79$), suggest similar sources and transport pathways (Figures 2 and 4). In this sense, the good agreement between the organic and inorganic tracers and the EDC dust and iron records, together with the results from $^{232}Th/^{230}Th$ analysis, imply that the supply of lithogenic material to our site is dominated by changes in the eolian input of terrigenous material through time. However, in some intervals additional sources (e.g., IRD) may have occasionally contributed to increase the supply of lithogenic material (Figure 2e), and hence of Fe [*Raiswell et al.*, 2006; *Smith et al.*, 2007; *Walter et al.*, 2000]. The relative importance of the redistribution of lithogenic material by surface currents and intermediate waters, that could eventually return to the surface by upwelling [*Blain et al.*, 2007], is difficult to evaluate. However, eolian supply is a more likely source of lithogenic material in the core site, as the potential chemical interactions that may have affected the organic and inorganic tracers during transport are bound to be less important during eolian transport than in the case of oceanic recirculation. Therefore, we conclude that an eolian source of lithogenic material (and hence of Fe) explains more simply the clear correlation observed between the n-alkanes and the inorganic tracers, however, in some intervals a contribution from other sources (e.g., IRD) cannot be totally discarded.

[19] By considering that lithogenic material is supplied by wind, we can give a quantitative estimation of the flux of dust to the ocean over the last 330 ka (Figure 3c), providing a better characterization of South American dust flux. We observe a clear G/IG dust flux variability of around 1 g m^{-2} a^{-1} of dust (50 mg m^{-2} a^{-1} of iron) for interglacial periods, to around 4–5 g m^{-2} a^{-1} (200 mg m^{-2} $a^{-1}$of iron) for glacial stages. This is in good agreement with other Fe reconstructions in the region [*Kumar et al.*, 1995], and confirms previous suggestions pointing to a 4 to fivefold increase in South American dust source strength during glacial stages [*Kumar et al.*, 1995; *Lambert et al.*, 2008]. This G/IG variability falls well within the Dirtmap inventory estimates for the source region [*Kohfeld and Harrison*, 2001] and represents a southwestern marine end-member of South American dust flux variability. In this sense, it is interesting to note that our glacial value is almost ten times

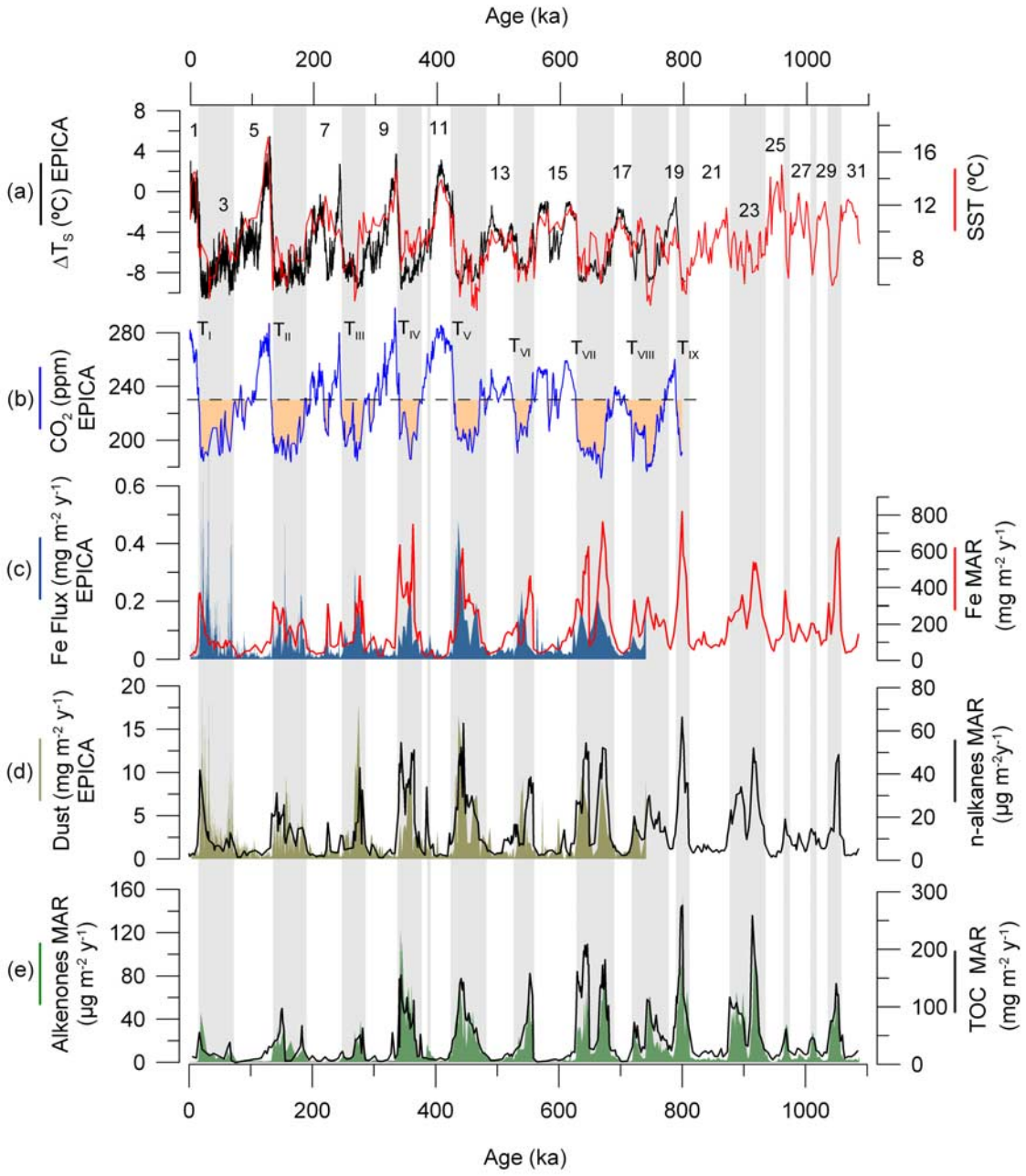

Figure 7. Comparison of the marine and terrestrial records over the last 1.1 Ma. (a) Temperature reconstruction from EPICA ice cores (black) [*Jouzel et al.*, 2007] and alkenone-based SST from Site PS2489-2/ODP1090 (red). MIS are shown for reference. (b) Atmospheric CO_2 concentrations from the EPICA ice cores [*Luthi et al.*, 2008; *Petit et al.*, 1999; *Siegenthaler et al.*, 2005]. Dashed line indicates the CO_2 level when productivity starts to increase above the average interglacial value. Filled area illustrates CO_2 concentrations below 230 ppmv. Glacial terminations are shown for reference. (c) EPICA Fe flux (blue) and Site PS2489-2/ODP1090 Fe flux (red). (d) EPICA insoluble dust (light brown) and Site PS2489-2/ODP1090 long-chain odd carbon-numbered n-alkanes (C_{23-33}) mass accumulation rate (MAR) (blue). (e) Site PS2489-2/ODP1090 C_{37} alkenones MAR (green) and TOC MAR [*Diekmann and Kuhn*, 2002] (black). Shaded areas highlight the high-productivity intervals when alkenones MAR are three times higher than the average interglacial value. The age model was obtained by correlation of marine and continental temperature profiles (see section 2.2).

higher than the estimations from dust deposition models for the site location [*Jickells et al.*, 2005; *Mahowald et al.*, 2006] suggesting that model estimations may be underestimating dust (and hence Fe) supply to the study location during glacial times.

[20] The observed G/IG variability in dust deposition observed in our record is higher than the 2 to 2.5-fold increase recently found in the equatorial Pacific [*Winckler et al.*, 2008] also estimated by $^{232}Th/^{230}Th$. This highlights the regional dissimilarities in South American dust source regions, suggesting a key role for local processes occurring in Patagonia, probably related to the advance of the Patagonian ice sheet or exposure of the Patagonian shelf, in amplifying dust generation with respect to the equatorial Pacific dust sources [*Ridgwell and Watson*, 2002; *Winckler et al.*, 2008]. However, our data indicate that this process cannot explain the 25-fold increase in dust fluxes observed in the Antarctic records. In this sense, our dust (and also SST) estimates are consistent with the mechanism recently proposed by *Lambert et al.* [2008] to explain the 25-fold increase in dust fluxes over Antarctica that involve a progressive coupling between Antarctica and lower latitudes during cold stages.

[21] Our long-term multiproxy reconstruction of dust inputs provides evidence from independent proxies of an increase in the supply of lithogenic material in each of the glacial stages of the last 1.1 Ma (Figure 2). Moreover, it reveals a first-order similarity of dust (n-alkanes) supply with the global ice volume record (Figure 5a) when the former is plotted in a logarithmic scale (e.g., $\delta^{18}O$/n-alkanes, $r^2 = 0.60$) (Figure 6). This suggests that the link between eolian dust transport in the Southern Hemisphere and the Pleistocene glaciations documented in EDC for the past 800 ka [*Lambert et al.*, 2008] can be extended back to 1.1 Ma. The increased dust deposition at site PS2489-2/ODP1090 is probably reflecting, as in the case of Antarctic ice cores, an increase both in the westerly winds strength and South American aridity during glacial stages. Moreover, since site PS2489-2/ODP1090 is located north of the zone of maximum westerly wind stress, our data are also consistent with a northward migration of the westerly winds belt during glacial stages. This process is of particular interest as according to several models, it is one of the critical physical mechanisms in the regulation of the deepwater ventilation around Antarctica, and hence of atmospheric CO_2 [*Toggweiler et al.*, 2006]. However, from our data we cannot distinguish the relative influence of changes in South American aridity, wind intensity and westerly wind belt position in the supply of dust to site PS2489-2/ODP1090.

3.2. Biological Response to Recurrent Iron Fertilization

[22] Our data provide evidence from different proxies of increased export production in the subantarctic South Atlantic during the late and mid Pleistocene glacial periods (Figures 2, 5, and 7). Moreover, the good agreement observed between Fe, alkenones and TOC concentrations and MAR across the entire record (Figures 2, 4, and 7) suggests that the process of iron fertilization of marine biota has been a recurrent mechanism operating in the subantarctic region during glacial stages over the last 1.1 Ma. From our data we cannot evaluate the relative effect of other factors that may have potentially influenced export production, such as an increase in the supply of macronutrients (N, P) from a glacial increase in wind-driven upwelling in the Subantarctic Zone (SZ). However, beyond this considerations that will be addressed by currently ongoing studies (e.g., $\delta^{15}N$), the good agreement between our proxies suggest a major effect of micronutrients (e.g., Fe) in modulating export production in the SZ over the last 1.1 Ma.

[23] In addition to the organic proxies (alkenones and TOC), authigenic U (U_{Auth}) and Re concentration profiles provide additional support for increased export production during glacial times (Figure 2g). The significant enrichment of U_{Auth} and Re indicates the unequivocal existence of suboxic conditions in PS2489-2/ODP1090 sediments during glacial periods [*Crusius and Thomson*, 2000]. This data alone cannot discern if suboxic conditions were created by elevated respiration as a consequence of the high export production or by lower oxygen concentrations in bottom waters due to changes in deep ocean circulation [*Anderson et al.*, 2002]. However, the results of the U_{Auth} compilation for the subantarctic Atlantic during the LGM by *Chase et al.* [2001], and the good correlation of our U_{Auth} and Re profiles with TOC and alkenones, suggest that the suboxic conditions found in our record during glacial times are consequence of the increased export production.

[24] An interesting feature observed in all the glacial periods is that the increase in export productivity observed during glacial stages is exponential rather than linear (Figures 5c and 6d). We suggest that this is because export production is driven mainly by changes in the supply of iron by dust, which is known to be exponentially correlated with global ice volume (Figures 5a and 6c) [*Lambert et al.*, 2008]. In this sense, export productivity at the beginning of the glacial period rises marginally and increases exponentially to reach the highest values when full glacial conditions are developed (Figures 5 and 7). This implies that changes in export production in the SZ are nonlinearly, but exponentially, correlated with the changes in atmospheric CO_2 levels (Figures 5c and 6d). This observation suggests that the potential of changes in the biological pump for decreasing atmospheric CO_2 concentrations was more important during glacial maxima than at the beginning of the glaciations when the increase in export production was in comparison very low. Actually, a common feature to all of the glacial intervals is that export production experiences a significant increase over the average interglacial value only once the CO_2 concentrations are ca. 230 ppmv, that is, more than 50 ppmv lower than during interglacials (Figure 7). According to these observations we suggest that the effect of the initial increase in export production on atmospheric CO_2 was probably minimal, and hence that the argument proposed for the last glacial cycle [*Kohfeld et al.*, 2005] that iron fertilization could only explain at most the last part of the CO_2 drawdown (up to 40–50 ppmv from our data in Figure 7), can be extended for other glacial stages of the late Pleistocene.

[25] On the long-term, TOC and alkenones MAR show higher levels of export production during glacial stages

between MIS 10 and 24. This is probably as a consequence of the higher iron inputs during these intervals (Figure 7c). However, this is not coincident with any significant change in atmospheric CO_2 concentrations. In this respect, it is interesting to note the higher interglacial export production observed prior to 400 ka (Figure 5c). Although in this case it is coincident with the decrease in the amplitude of atmospheric CO_2 concentrations, the absolute change in interglacial export production is very small compared to the amplitude of the G/IG variations, and it is unlikely that it could explain the lower CO_2 values prior to 400 ka. In this sense, our results suggest that the change in amplitude of atmospheric CO_2 concentrations, as well as the initial CO_2 drawdown during glacial stages, could be probably better explained by changes in the physical mechanisms than by variations in the strength of the biological pump. Although these results may be in a way representative of other regions of the ocean where productivity is also driven by iron inputs, we recognize that the situation may have been different in other areas of the world ocean. In this sense further studies are needed to confirm the hypothesis presented here concerning the long-term evolution of global export production and its relationship to atmospheric CO_2 changes.

3.3. Sea Surface Temperature Changes in the Subantarctic Atlantic

[26] The alkenone-based SST reconstruction presented here provides the strongest evidence to date that subantarctic SST covaried with Antarctic air temperature over the past 800 ka (Figure 7). This paleotemperature reconstruction represents an improvement of previous SST estimates from Site PS2489-2/ODP1090 on the basis of planktonic foraminiferal transfer functions [*Becquey and Gersonde*, 2002, 2003] that appeared to be partially biased by dissolution in some intervals. The G/IG temperature variability of the alkenone reconstruction is relatively similar to the foraminiferal transfer function [*Becquey and Gersonde*, 2002, 2003], especially during the last 600 ka (see Figure S3 in the Auxiliary Material). Major differences occur in those intervals with evidence of foraminiferal dissolution (e.g., MIS11). However, absolute values from alkenone temperature estimates are higher than from foraminifera, a fact that has been noticed in other records worldwide, especially in high-latitude ocean settings [*Bard*, 2001; *de Vernal et al.*, 2006; *Lee et al.*, 2001; *Sikes et al.*, 2002]. Several causes have been invoked to account for this differences such as changes in the seasonality, differences in the water depth signal recorded by each proxy, or variations in the stratification and thermal diffusion in the upper water column [*de Vernal et al.*, 2006]. Beyond these considerations, both proxies start to differ more significantly prior to 900 ka, where foraminiferal estimates show very small G/IG variability. This may be explained by the increase in the foraminiferal fragmentation ratio around this period [*Becquey and Gersonde*, 2002], which might have caused a relative enrichment in *Neogloboquadrina pachiderma sin*. during interglacials, and hence a slight underestimation of interglacial temperatures beyond 900 ka.

[27] The variability in the strength of interglacials observed in the EDC temperature was explained as the result of changes in orbital parameters [*Jouzel et al.*, 2007]. Thus, when obliquity maxima are in phase with precession minima, their combined effects in solar radiation induce a strong interglacial, while when they are in antiphase the result is a weaker interglacial [*Jouzel et al.*, 2007]. Our data are in good agreement with this hypothesis, and provide new insights into the evolution of these mechanisms back to MIS 31 (see Figures S4 and S5 of the Auxiliary Material). Interglacial SSTs beyond the Mid-Brunhes Event (MBE; ca. 400 ka) are colder than in the most recent interglacials (MIS 1, 5.5, 7.5, 9.3 and 11.3), with the exception of MIS 25. Site PS2489-2/1090 SST power spectra is, as the δDT record [*Jouzel et al.*, 2007], dominated by a periodicity of 100 ka and present a strong obliquity component, while the influence of precession is only apparent in the last 400 ka (Figure S4 of the Auxiliary Material). The relative strength of the orbital parameters appears to increase through time in our record, in good agreement with the EDC record [*Jouzel et al.*, 2007]. The similarity in the spectral features of both records supports previous suggestions pointing at ocean circulation feedbacks as a mechanism for transferring the high-latitude obliquity signal toward the tropics [*Jouzel et al.*, 2007; *Lee and Poulsen*, 2006].

[28] SST also exhibits clear millennial scale variability during glacial stages (Figure 7a). The sample resolution is too low to resolve submillennial events but larger suborbital variability in SST is clearly recorded. This would offer a marine counterpart to the EDC temperature profile supporting the view that marine processes involved in deepwater formation are key for the onset of glacial climate instabilities [*Jouzel et al.*, 2007]. Interestingly, the new data back to 1.1 Ma show that this high-frequency variability was also present in glacial stages beyond MIS 19.

[29] The high correlation of the alkenone-SST to the EDC temperature reconstruction over the entire span of the ice core record (i.e., 800 ka) implies that Antarctic atmospheric temperatures and atmospheric CO_2 concentrations are closely linked to changes in Southern Ocean surface temperatures. This confirms previous hypotheses [*Sigman et al.*, 2004; *Stephens and Keeling*, 2000; *Toggweiler et al.*, 2006] that invoke oceanic processes to explain the close connection between atmospheric temperatures and CO_2. In support of this interpretation, before the MBE, our alkenone SST profile shows lower amplitude of G/IG oscillations (also apparent in the foraminiferal SST) in good agreement with the EDC temperature and coincident with lower interglacial atmospheric CO_2 concentrations (Figure 7). These colder interglacial temperatures suggest an increased Antarctic sea ice cover, and possibly an enhanced water column stratification in the SO during interglacial stages before the MBE (MIS 13, 15 17 and 19) compared to more recent integlacials (MIS 1, 5, 7, 9 and 11). According to model studies [*Francois et al.*, 1997; *Stephens and Keeling*, 2000], such changes may have resulted in reduced deepwater ventilation of CO_2-rich waters and/or in reduced ocean-atmosphere gas exchange rates around Antarctica during interglacial stages prior to the MBE, which could be one mechanism to explain the lower interglacial CO_2 levels observed in the EDC ice

cores during this period (400–800 ka). However, further studies are needed to determine the extension and seasonal distribution of Antarctic sea ice cover, as well as the stratification state of the Southern Ocean during interglacial stages prior to the MBE.

[30] Colder pre-MBE interglacial temperature regimes in the present subantarctic realm could be related to more northward located westerlies compared with post-MBE interglacials. This might have acted as a positive feedback in the mechanism described above involving sea ice and water column stratification to explain the lower interglacial CO_2 levels during this period (400–800 ka) [*Toggweiler et al.*, 2006; *Toggweiler and Russell*, 2008]. In this sense, the slightly higher interglacial n-alkanes concentrations and MAR observed between 400 and 800 ka (Figures 5 and 7) may be interpreted as an evidence of this mechanism. However, as mentioned in section 3.1, other factors such as changes in wind intensity or South American aridity, may have also contributed to explain the slightly increased dust deposition at Site PS2489-2/ODP1090 during interglacial stages before the MBE.

4. Conclusions

[31] The data set presented here contributes from a combined marine-terrestrial perspective to shed light into the importance the Southern Ocean processes in the regulation of atmospheric CO_2 at orbital timescales over the last 1.1 Ma. We show that dust and iron inputs to the ocean and marine productivity are closely coupled over the last 1.1 Ma and hence, that the process of iron fertilization of marine biota has been operating in the subantarctic region over this time span. However, this process can only explain a fraction of atmospheric CO_2 changes occurring at glacial maxima (up to around 40–50 ppmv from our data) in glacial stages back to 800 ka. Our alkenone SST reconstruction, documents that atmospheric and Southern Ocean processes are closely linked over the last 800 ka and probably beyond this age. This has occurred in parallel with other processes potentially involved in the regulation of atmospheric CO_2 concentrations, such as the movements of the westerly wind belt, and changes in sea ice extent and surface water stratification. The relative timing of the different processes suggests that the initial CO_2 decrease during the different climate cycles as well as the change in the amplitude of the CO_2 cycles observed around 400 ka, were most likely driven by physical processes, possibly related to changes in Southern Ocean sea ice extent, surface water stratification and westerly winds position rather than related to changes in the biological pump. This conclusion is supported by the fact that physical mechanisms can be considered in a way self sustaining with respect to the CO_2 changes. Thus, a physically based transition (driven by changes in temperature, stratification, sea ice, and shifts in the westerlies) can be initiated by an internal disturbance and will tend to keep going until the deep ocean cannot hold or give up any more CO_2. While in the case of the biological pump its effect on atmospheric CO_2 is dependent on the increase in iron supply, which according to this study constrains its potential contribution to the glacial maxima. Therefore, we concur with previous proposals based on records with shorter time spans or modeling studies, that the explanation of the G/IG variations in atmospheric CO_2 concentrations requires consideration of the relative timing and intensity of the interaction of multiple physical and biogeochemical processes through time.

[32] **Acknowledgments.** We thank Bob Anderson and J. R. Toggweiler for reviewing the manuscript and providing helpful suggestions for the improvement of the final version of the paper. We acknowledge the Integrated Ocean Drilling Program (IODP) and the Polarstern core repository from the Alfred Wegener Institute (AWI) for providing the samples used in this study. We thank the Spanish "Ministerio de Educación y Ciencia" for a Ph.D. grant to AM-G and project POL2006-02999. This work is a contribution to the European Project for Ice Coring in Antarctica (EPICA-MIS), a joint ESF/EC scientific program, funded by the European Commission and by national contributions from Belgium, Denmark, France, Germany, Italy, the Netherlands, Norway, Sweden, Switzerland, and the United Kingdom. This is EPICA publication number 214. Thanks are also given to I. Vöge, T. Roeske, S. Kretschmer, O. Lechtenfeld, and N. Moraleda for their help in the laboratory analysis and to P. G. Mortyn, S. Rossi, J. Carraquiry, M. Martínez-Botí, G. Martínez-Méndez, and M. Escala for helpful discussions.

References

Abelmann, A., R. Gersonde, G. Cortese, G. Kuhn, and V. Smetacek (2006), Extensive phytoplankton blooms in the Atlantic sector of the glacial Southern Ocean, *Paleoceanography*, *21*(1), PA1013,doi:10.1029/2005PA001199.

Anderson, R. F., Z. Chase, M. Q. Fleisher, and J. Sachs (2002), The Southern Ocean's biological pump during the Last Glacial Maximum, *Deep Sea Res., Part II*, *49*(9–10), 1909–1938, doi:10.1016/S0967-0645(02)00018-8.

Anderson, R. F., M. Q. Fleisher, and Y. Lao (2006), Glacial-interglacial variability in the delivery of dust to the central equatorial Pacific Ocean, *Earth Planet. Sci. Lett.*, *242*(3–4), 406–414, doi:10.1016/j.epsl.2005.11.061.

Barbante, C., T. Bellomi, G. Mezzadri, P. Cescon, G. Scarponi, C. Morel, S. Jay, K. Van De Velde, C. Ferrari, and C. F. Boutron (1997), Direct determination of heavy metals at picogram per gram levels in Greenland and Antarctic snow by double focusing inductively coupled plasma mass spectrometry, *J. Anal. At. Spectrom.*, *12*(9), 925–931, doi:10.1039/a701686g.

Bard, E. (2001), Comparison of alkenone estimates with other paleotemperature proxies, *Geochem. Geophys. Geosyst.*, *2*(1), 1002, doi:10.1029/2000GC000050.

Bard, E., F. Rostek, J. L. Turon, and S. Gendreau (2000), Hydrological impact of Heinrich events in the subtropical northeast Atlantic, *Science*, *289*(5483), 1321–1324, doi:10.1126/science.289.5483.1321.

Becquey, S., and R. Gersonde (2002), Past hydrographic and climatic changes in the Subantarctic Zone of the South Atlantic: The Pleistocene record from ODP Site 1090, *Palaeogeogr. Palaeoclimatol. Palaeoecol.*, *182*(3–4), 221–239, doi:10.1016/S0031-0182(01)00497-7.

Becquey, S., and R. Gersonde (2003), A 0.55-Ma paleotemperature record from the Subantarctic Zone: Implications for Antarctic Circumpolar Current development, *Paleoceanography*, *18*(1), 1014, doi:10.1029/2000PA000576.

Belkin, I. M., and A. L. Gordon (1996), Southern Ocean fronts from the Greenwich meridian to Tasmania, *J. Geophys. Res.*, *101*(C2), 3675–3696, doi:10.1029/95JC02750.

Bendle, J., and A. Rosell-Mele (2004), Distributions of U^{K}_{37} and U^{K}_{37}' in the surface waters and sediments of the Nordic Seas: Implications for paleoceanography, *Geochem. Geophys. Geosyst.*, *5*, Q11013, doi:10.1029/2004GC000741.

Blain, S., et al. (2007), Effect of natural iron fertilization on carbon sequestration in the Southern Ocean, *Nature*, *446*(7139), 1070–1071, doi:10.1038/nature05700.

Boyd, P. W., et al. (2007), Mesoscale iron enrichment experiments 1993–2005: Synthesis and future directions, *Science*, *315*(5812), 612–617, doi:10.1126/science.1131669.

Brassell, S. C., G. Eglinton, I. T. Marlowe, U. Pflaumann, and M. Sarnthein (1986), Molecular stratigraphy: A new tool for climatic assessment, *Nature*, *320*(6058), 129–133, doi:10.1038/320129a0.

Brovkin, V., A. Ganopolski, D. Archer, and S. Rahmstorf (2007), Lowering of glacial atmospheric CO_2 in response to changes in oceanic circulation and marine biogeochemistry, *Paleoceanography*, *22*, PA4202, doi:10.1029/2006PA001380.

Buesseler, K. O., and P. W. Boyd (2003), Will ocean fertilization work?, *Science*, *300*(5616), 67–68, doi:10.1126/science.1082959.

Buesseler, K. O., et al. (2008), Ocean iron fertilization: Moving forward in a sea of uncertainty, *Science*, *319*, 162, doi:10.1126/science.1154305.

Calvert, S. E., and T. F. Pedersen (2007), Elemental proxies for palaeoclimatic and palaeoceanographic variability in marine sediments: Interpretation and application, in *Proxies in Late Cenozoic Paleoceanography*, edited by C. Hillaire-Marcel and A. de Vernal, pp. 567–644, Elsevier, Amsterdam, Netherlands.

Chase, Z., R. F. Anderson, and M. Q. Fleisher (2001), Evidence from authigenic uranium for increased productivity of the glacial Subantarctic Ocean, *Paleoceanography*, *16*(5), 468–478, doi:10.1029/2000PA000542.

Chisholm, S. W., P. G. Falkowski, and J. J. Cullen (2001), Oceans: Dis-crediting ocean fertilization, *Science*, *294*(5541), 309–310, doi:10.1126/science.1065349.

Chisholm, S. W., P. G. Falkowski, and J. J. Cullen (2002), Is ocean fertilization credible and creditable? Response, *Science*, *296*(5567), 467–468, doi:10.1126/science.296.5567.467b.

Comiso, J. C. (2003), Large scale characteristics and variability of the global sea ice cover, in *Sea Ice an Introduction to its Physics, Biology, Chemistry and Geology*, edited by D. Thomas and G. S. Diekmann, pp. 112–142, Blackwell, Oxford, UK.

Crusius, J., and J. Thomson (2000), Comparative behavior of authigenic Re, U, and Mo during reoxidation and subsequent long-term burial in marine sediments, *Geochim. Cosmochim. Acta*, *64*(13), 2233–2242, doi:10.1016/S0016-7037(99)00433-0.

Delmonte, B., J. R. Petit, and V. Maggi (2002), LGM-Holocene changes and Holocene millennial-scale oscillations of dust particles in the EPICA Dome C ice core, East Antarctica, *Ann. Glaciol.*, *35*(1), 306–312, doi:10.3189/172756402781816843.

de Vernal, A., A. Rosell-Melé, M. Kucera, C. Hillaire-Marcel, F. Eynaud, M. Weinelt, T. Dokken, and M. Kageyama (2006), Comparing proxies for the reconstruction of LGM sea-surface conditions in the northern North Atlantic, *Quat. Sci. Rev.*, *25*(21–22), 2820–2834, doi:10.1016/j.quascirev.2006.06.006.

Diekmann, B., and G. Kuhn (2002), Sedimentary record of the mid-Pleistocene climate transition in the southeastern South Atlantic (ODP Site 1090), *Palaeogeogr. Palaeoclimatol. Palaeoecol.*, *182*(3–4), 241–258, doi:10.1016/S0031-0182(01)00498-9.

Eglinton, G., and R. J. Hamilton (1967), Leaf epicuticular waxes, *Science*, *156*(3780), 1322–1335, doi:10.1126/science.156.3780.1322.

EPICA Community Members (2004), Eight glacial cycles from an Antarctic ice core, *Nature*, *429*(6992), 623–628, doi:10.1038/nature02599.

Francois, R., M. A. Altabet, E. F. Yu, D. M. Sigman, M. P. Bacon, M. Frank, G. Bohrmann, G. Bareille, and L. D. Labeyrie (1997), Contribution of Southern Ocean surface-water stratification to low atmospheric CO_2 concentrations during the last glacial period, *Nature*, *389*(6654), 929–935, doi:10.1038/40073.

Francois, R., M. Frank, M. M. R. van der Loeff, and M. P. Bacon (2004), Th-230 normalization: An essential tool for interpreting sedimentary fluxes during the late Quaternary, *Paleoceanography*, *19*(1), PA1018, doi:10.1029/2003PA000939.

Frank, M., R. Gersonde, M. R. van der Loeff, G. Bohrmann, C. C. Nurnberg, P. W. Kubik, M. Suter, and A. Mangini (2000), Similar glacial and interglacial export bioproductivity in the Atlantic sector of the Southern Ocean: Multiproxy evidence and implications for glacial atmospheric CO_2, *Paleoceanography*, *15*(6), 642–658, doi:10.1029/2000PA000497.

Gabrielli, P., C. Barbante, C. F. Boutron, G. Cozzi, V. Gaspari, F. Planchon, C. Ferrari, C. Turetta, S. Hong, and P. Cescon (2005), Variations in atmospheric trace elements in Dome C (East Antarctica) ice over the last two climatic cycles, *Atmos. Environ.*, *39*, 6420–6429, doi:10.1016/j.atmosenv.2005.07.025.

Gaspari, V., C. Barbante, G. Cozzi, P. Cescon, C. F. Boutron, P. Gabrielli, G. Capodaglio, C. Ferrari, J. R. Petit, and B. Delmonte (2006), Atmospheric iron fluxes over the last deglaciation: Climatic implications, *Geophys. Res. Lett.*, *33*(3), L03704, doi:10.1029/2005GL024352.

Geibert, W., M. M. R. van der Loeff, R. Usbeck, R. Gersonde, G. Kuhn, and J. Seeberg-Elverfeldt (2005), Quantifying the opal belt in the Atlantic and southeast Pacific sector of the Southern Ocean by means of Th-230 normalization, *Global Biogeochem. Cycles*, *19*(4), GB4001, doi:10.1029/2005GB002465.

Gersonde, R., et al. (1999), *Proceedings of the Ocean Drilling Program Initial Reports*, Ocean Drill. Program, College Station, Tex.

Gersonde, R., X. Crosta, A. Abelmann, and L. Armand (2005), Sea-surface temperature and sea lee distribution of the Southern Ocean at the EPILOG Last Glacial Maximum: A circum-Antarctic view based on siliceous microfossil records, *Quat. Sci. Rev.*, *24*(7–9), 869–896, doi:10.1016/j.quascirev.2004.07.015.

Hansen, R. G., and E. J. Ring (1983), The preparation and certification of a uranium reference material, *Report M84, 8 S, Council of Mineral Technology*, Randburg, South Africa.

Horwitz, E. P., M. L. Dietz, R. Chiarizia, H. Diamond, A. M. Essling, and D. Graczyk (1992), Separation and preconcentration of uranium from acidic media by extraction chromatography, *Anal. Chim. Acta*, *266*(1), 25–37, doi:10.1016/0003-2670(92)85276-C.

Hulton, N. R. J., R. S. Purves, R. D. McCulloch, D. E. Sugden, and M. J. Bentley (2002), The Last Glacial Maximum and deglaciation in southern South America, *Quat. Sci. Rev.*, *21*(1–3), 233–241, doi:10.1016/S0277-3791(01)00103-2.

Jickells, T. D., et al. (2005), Global iron connections between desert dust, ocean biogeochemistry, and climate, *Science*, *308*(5718), 67–71, doi:10.1126/science.1105959.

Johnson, K. S., and D. M. Karl (2002), Is ocean fertilization credible and creditable?, *Science*, *296*(5567), 467–468, doi:10.1126/science.296.5567.467b.

Jouzel, J., et al. (2007), Orbital and millennial Antarctic climate variability over the past 800,000 years, *Science*, *317*(5839), 793–796, doi:10.1126/science.1141038.

Kohfeld, K. E., and S. P. Harrison (2001), DIRTMAP: The geological record of dust, *Earth Sci. Rev.*, *54*(1–3), 81–114, doi:10.1016/S0012-8252(01)00042-3.

Kohfeld, K. E., C. Le Quere, S. P. Harrison, and R. F. Anderson (2005), Role of marine biology in glacial-interglacial CO_2 cycles, *Science*, *308*(5718), 74–78, doi:10.1126/science.1105375.

Kohler, P., H. Fischer, G. Munhoven, and R. E. Zeebe (2005), Quantitative interpretation of atmospheric carbon records over the last glacial termination, *Global Biogeochem. Cycles*, *19*(4), GB4020, doi:10.1029/2004GB002345.

Kornilova, O., and A. Rosell-Mele (2003), Application of microwave-assisted extraction to the analysis of biomarker climate proxies in marine sediments, *Org. Geochem.*, *34*(11), 1517–1523, doi:10.1016/S0146-6380(03)00155-4.

Kumar, N., R. F. Anderson, R. A. Mortlock, P. N. Froelich, P. Kubik, B. Dittrichhannen, and M. Suter (1995), Increased biological productivity and export production in the glacial Southern Ocean, *Nature*, *378*(6558), 675–680, doi:10.1038/378675a0.

Lambert, F., B. Delmonte, J. R. Petit, M. Bigler, P. R. Kaufmann, M. A. Hutterli, T. F. Stocker, U. Ruth, J. P. Steffensen, and V. Maggi (2008), Dust-climate couplings over the past 800,000 years from the EPICA Dome C ice core, *Nature*, *452*(7187), 616–619, doi:10.1038/nature06763.

Latimer, J. C., and G. M. Filippelli (2007), Sedimentary iron records from the Cape Basin, *Deep Sea Res., Part II*, *54*(21–22), 2422, doi:10.1016/j.dsr2.2007.07.022.

Latimer, J. C., G. M. Filippelli, I. L. Hendy, J. D. Gleason, and J. D. Blum (2006), Glacial-interglacial terrigenous provenance in the southeastern Atlantic Ocean: The importance of deep-water sources and surface currents, *Geology*, *34*(7), 545–548, doi:10.1130/G22252.1.

Lee, K. E., N. C. Slowey, and T. D. Herbert (2001), Glacial sea surface temperatures in the subtropical North Pacific: A comparison of $U^{K}_{37}{}'$, $\delta^{18}O$, and foraminiferal assemblage temperature estimates, *Paleoceanography*, *16*(3), 268–279, doi:10.1029/1999PA000493.

Lee, S. Y., and C. J. Poulsen (2006), Sea ice control of Plio-Pleistocene tropical Pacific climate evolution, *Earth Planet. Sci. Lett.*, *248*(1–2), 253–262, doi:10.1016/j.epsl.2006.05.030.

Lisiecki, L. E., and M. E. Raymo (2005), A Pliocene-Pleistocene stack of 57 globally distributed benthic delta O-18 records, *Paleoceanography*, *20*(1), PA1003, doi:10.1029/2004PA001071.

Luthi, D., et al. (2008), High-resolution carbon dioxide concentration record 650,000–800,000 years before present, *Nature*, *453*(7193), 379–382, doi:10.1038/nature06949.

Mahowald, N. M., D. R. Muhs, S. Levis, P. J. Rasch, M. Yoshioka, C. S. Zender, and C. Luo (2006), Change in atmospheric mineral aerosols in response to climate: Last glacial period, preindustrial, modern, and doubled carbon dioxide climates, *J. Geophys. Res.*, *111*, D10202, doi:10.1029/2005JD006653.

Martin, J. (1990), Glacial-interglacial CO2 change: The iron hypothesis, *Paleoceanography*, *5*(1), 1–13, doi:10.1029/PA005i001p00001.

McClymont, E. L., A. Martinez-Garcia, and A. Rosell-Mele (2007), Benefits of freeze-drying sediments for the analysis of total chlorins and alkenone concentrations in marine sediments, *Org. Geochem.*, *38*(6), 1002–1007, doi:10.1016/j.orggeochem.2007.01.006.

Paillard, D., L. Labeyrie, and P. Yiou (1996), Macintosh program performs time-series ana-

lysis, *Eos Trans. AGU*, *77*, 379, doi:10.1029/96EO00259.

Parrenin, F., et al. (2007), The EDC3 chronology for the EPICA dome C ice core, *Clim. Past*, *3*(3), 485–497.

Petit, J. R., et al. (1999), Climate and atmospheric history of the past 420,000 years from the Vostok ice core, Antarctica, *Nature*, *399*(6735), 429–436, doi:10.1038/20859.

Planchon, F. A. M., C. F. Boutron, C. Barbante, E. W. Wolff, G. Cozzi, V. Gaspari, C. P. Ferrari, and P. Cescon (2001), Ultrasensitive determination of heavy metals at the subpicogram per gram level in ultraclean Antarctic snow samples by inductively coupled plasma sector field mass spectrometry, *Anal. Chim. Acta*, *450*(1–2), 193–205, doi:10.1016/S0003-2670(01)01379-4.

Prahl, F. G., and S. G. Wakeham (1987), Calibration of unsaturation patterns in long-chain ketone compositions for paleotemperature assessment, *Nature*, *330*(6146), 367–369, doi:10.1038/330367a0.

Raiswell, R., M. Tranter, L. G. Benning, M. Siegert, R. De'ath, P. Huybrechts, and T. Payne (2006), Contributions from glacially derived sediment to the global iron (oxyhydr)oxide cycle: Implications for iron delivery to the oceans, *Geochim. Cosmochim. Acta*, *70*(11), 2765–2780, doi:10.1016/j.gca.2005.12.027.

Rashid, H., and E. Grosjean (2006), Detecting the source of Heinrich layers: An organic geochemical study, *Paleoceanography*, *21*(3), PA3014, doi:10.1029/2005PA001240.

Ridgwell, A. J., and A. J. Watson (2002), Feedback between aeolian dust, climate, and atmospheric CO_2 in glacial time, *Paleoceanography*, *17*(4), 1059, doi:10.1029/2001PA000729.

Rosell-Mele, A. (1998), Interhemispheric appraisal of the value of alkenone indices as temperature and salinity proxies in high-latitude locations, *Paleoceanography*, *13*(6), 694–703, doi:10.1029/98PA02355.

Rosell-Mele, A., G. Eglinton, U. Pflaumann, and M. Sarnthein (1995), Atlantic core-top calibration of the U^{K}_{37} index as a sea-surface palaeotemperature indicator, *Geochim. Cosmochim. Acta*, *59*(15), 3099–3107, doi:10.1016/0016-7037(95)00199-A.

Rosell-Mele, A., M. A. Maslin, J. R. Maxwell, and P. Schaeffer (1997), Biomarker evidence for "Heinrich" events, *Geochim. Cosmochim. Acta*, *61*(8), 1671–1678, doi:10.1016/S0016-7037(97)00046-X.

Rosell-Mele, A., et al. (2001), Precision of the current methods to measure the alkenone proxy U^{K}_{37}' and absolute alkenone abundance in sediments: Results of an interlaboratory comparison study, *Geochem. Geophys. Geosyst.*, *2(7), 1046, doi:10.1029/2000GC000141.*

Sayles, F. L., W. R. Martin, Z. Chase, and R. F. Anderson (2001), Benthic remineralization and burial of biogenic SiO_2, $CaCO_3$, organic carbon, and detrital material in the Southern Ocean along a transect at 170 degrees West, *Deep Sea Res., Part II*, *48*(19–20), 4323–4383, doi:10.1016/S0967-0645(01)00091-1.

Siegenthaler, U., et al. (2005), Stable carbon cycle-climate relationship during the late Pleistocene, *Science*, *310*(5752), 1313–1317, doi:10.1126/science.1120130.

Sigman, D. M., and E. A. Boyle (2000), Glacial/interglacial variations in atmospheric carbon dioxide, *Nature*, *407*(6806), 859–869, doi:10.1038/35038000.

Sigman, D. M., S. L. Jaccard, and G. H. Haug (2004), Polar ocean stratification in a cold climate, *Nature*, *428*(6978), 59–63, doi:10.1038/nature02357.

Sikes, E. L., W. R. Howard, H. L. Neil, and J. K. Volkman (2002), Glacial-interglacial sea surface temperature changes across the subtropical front east of New Zealand based on alkenone unsaturation ratios and foraminiferal assemblages, *Paleoceanography*, *17*(2), 1012, doi:10.1029/2001PA000640.

Simoneit, B. R. T. (1977), Organic matter in eolian dusts over the Atlantic Ocean, *Mar. Chem.*, *5*(4–6), 443–464, doi:10.1016/0304-4203(77)90034-2.

Smith, K. L. Jr., B. H. Robison, J. J. Helly, R. S. Kaufmann, H. A. Ruhl, T. J. Shaw, B. S. Twining, and M. Vernet (2007), Free-drifting icebergs: Hot spots of Chemical and biological enrichment in the Weddell Sea, *Science*, *317*(5837), 478–482, doi:10.1126/science.1142834.

Stephens, B. B., and R. F. Keeling (2000), The influence of Antarctic sea ice on glacial-interglacial CO_2 variations, *Nature*, *404*(6774), 171–174, doi:10.1038/35004556.

Toggweiler, J. R. (1999), Variation of atmospheric CO_2 by ventilation of the ocean's deepest water, *Paleoceanography*, *14*(5), 571–588, doi:10.1029/1999PA900033.

Toggweiler, J. R., and J. Russell (2008), Ocean circulation in a warming climate, *Nature*, *451*(7176), 286–288, doi:10.1038/nature06590.

Toggweiler, J. R., J. L. Russell, and S. R. Carson (2006), Midlatitude westerlies, atmospheric CO_2, and climate change during the ice ages, *Paleoceanography*, *21*(2), PA2005, doi:10.1029/2005PA001154.

Venz, K. A., and D. A. Hodell (2002), New evidence for changes in Plio-Pleistocene deep water circulation from Southern Ocean ODP Leg 177 Site 1090, *Palaeogeogr. Palaeoclimatol. Palaeoecol.*, *182*(3–4), 197–220, doi:10.1016/S0031-0182(01)00496-5.

Walter, H. J., E. Hegner, B. Diekmann, G. Kuhn, and M. M. R. van der Loeff (2000), Provenance and transport of terrigenous sediment in the South Atlantic Ocean and their relations to glacial and interglacial cycles: Nd and Sr isotopic evidence, *Geochim. Cosmochim. Acta*, *64*(22), 3813–3827, doi:10.1016/S0016-7037(00)00476-2.

Watson, A. J., D. C. E. Bakker, A. J. Ridgwell, P. W. Boyd, and C. S. Law (2000), Effect of iron supply on Southern Ocean CO_2 uptake and implications for glacial atmospheric CO_2, *Nature*, *407*(6805), 730–733, doi:10.1038/35037561.

Winckler, G., R. F. Anderson, M. Q. Fleisher, D. McGee, and N. Mahowald (2008), Covariant glacial-interglacial dust fluxes in the equatorial Pacific and Antarctica, *Science*, *320*(5872), 93–96, doi:10.1126/science.1150595.

Wolff, E. W., et al. (2006), Southern Ocean sea ice extent, productivity and iron flux over the past eight glacial cycles, *Nature*, *440*(7083), 491–496, doi:10.1038/nature04614.

C. Barbante and V. Gaspari, Institute for the Dynamics of Environmental Processes, CNR, I-30123 Venice, Italy.

W. Geibert, School of Geosciences, University of Edinburgh, Edinburgh, UK.

R. Gersonde, Alfred Wegener Institute for Polar and Marine Research, D-27568 Bremerhaven, Germany.

A. Martínez-Garcia, Pere Masqué, and A. Rosell-Melé, Institut de Ciència i Tecnologia Ambientals, Universitat Autònoma de Barcelona, Bellaterra, Catalonia, E-08193, Spain. (antoni.rosell@uab.cat)